AGU PUBLICATIONS

Geophysical Research Letters

RESEARCH LETTER
10.1002/2016GL069188

Special Section:
First results from NASA's Magnetospheric Multiscale (MMS) Mission

Multispacecraft analysis of dipolarization fronts and associated whistler wave emissions using MMS data

H. Breuillard[1], O. Le Contel[1], A. Retino[1], A. Chasapis[2], T. Chust[1], L. Mirioni[1], D. B. Graham[3], F. D. Wilder[4], I. Cohen[5], A. Vaivads[3], Yu. V. Khotyaintsev[3], P.-A. Lindqvist[6], G. T. Marklund[6], J. L. Burch[7], R. B. Torbert[8], R. E. Ergun[4], K. A. Goodrich[4], J. Macri[8], J. Needell[8], M. Chutter[8], D. Rau[8], I. Dors[8], C. T. Russell[9], W. Magnes[10], R. J. Strangeway[9], K. R. Bromund[11], F. Plaschke[10], D. Fischer[10], H. K. Leinweber[9], B. J. Anderson[5], G. Le[11], J. A. Slavin[12], E. L. Kepko[11], W. Baumjohann[10], B. Mauk[3], S. A. Fuselier[13], and R. Nakamura[10]

[1]Laboratoire de Physique des Plasmas (LPP/CNRS UMR), Paris, France, [2]Department of Physics and Astronomy, University of Delaware, Newark, Delaware, USA, [3]Swedish Institute of Space Physics, Uppsala, Sweden, [4]LASP, University of Colorado, Boulder, Colorado, USA, [5]The Johns Hopkins University Applied Physics Laboratory, Laurel, Maryland, USA, [6]Alfven Laboratory, Royal Institute of Technology, Stockholm, Sweden, [7]Southwest Research Institute, San Antonio, TX, USA, [8]Space Science Center and Department of Physics, University of New Hampshire, Durham, New Hampshire, USA, [9]Institute of Geophysics and Planetary Physics, UCLA, Los Angeles, California, USA, [10]Space Research Institute (IWF), /Austrian Academy of Sciences, Graz, Austria, [11]NASA Goddard Space Flight Center, Greenbelt, Maryland, USA, [12]Department of Climate and Space Sciences and Engineering, University of Michigan, Ann Arbor, Michigan, USA, [13]Physics and Astronomy Department, University of Texas at San Antonio, Texas, USA

Key Points:
- Spatial dynamics of dipolarization fronts are below the ion gyroradius
- Associated whistler wave dynamics have a temporal scale of the order of the ion gyroperiod
- The nature of DFs and its implication on associated low-frequency waves is discussed

Correspondence to:
H. Breuillard,
hugo.breuillard@lpp.polytechnique.fr

Citation:
Breuillard, H., et al. (2016), Multispacecraft analysis of dipolarization fronts and associated whistler wave emissions using MMS data, *Geophys. Res. Lett.*, *43*, 7279–7286, doi:10.1002/2016GL069188.

Received 15 APR 2016
Accepted 23 MAY 2016
Accepted article online 8 JUN 2016
Published online 16 JUL 2016

Abstract Dipolarization fronts (DFs), embedded in bursty bulk flows, play a crucial role in Earth's plasma sheet dynamics because the energy input from the solar wind is partly dissipated in their vicinity. This dissipation is in the form of strong low-frequency waves that can heat and accelerate energetic electrons up to the high-latitude plasma sheet. However, the dynamics of DF propagation and associated low-frequency waves in the magnetotail are still under debate due to instrumental limitations and spacecraft separation distances. In May 2015 the Magnetospheric Multiscale (MMS) mission was in a string-of-pearls configuration with an average intersatellite distance of 160 km, which allows us to study in detail the microphysics of DFs. Thus, in this letter we employ MMS data to investigate the properties of dipolarization fronts propagating earthward and associated whistler mode wave emissions. We show that the spatial dynamics of DFs are below the ion gyroradius scale in this region (∼500 km), which can modify the dynamics of ions in the vicinity of the DF (e.g., making their motion nonadiabatic). We also show that whistler wave dynamics have a temporal scale of the order of the ion gyroperiod (a few seconds), indicating that the perpendicular temperature anisotropy can vary on such time scales.

1. Introduction

Transient fast flows of plasma are often observed for a large range of geocentric distances in Earth's magnetotail, from −5 to about −30 R_E [*Ohtani et al.*, 2004]. They are thought to be formed by reconnection of stretched field lines in the tail [*Runov et al.*, 2009; *Sitnov et al.*, 2009] and/or in interchange heads [*Pritchett and Coroniti*, 2011, 2013]. These bursty bulk flows (BBFs) are well correlated with substorm activity [see, e.g., *Juusola et al.*, 2011] and are an important mechanism of the flux transport in the tail [*Baumjohann*, 1993; *Baumjohann et al.*, 2002; *Volwerk et al.*, 2008]. BBFs propagating earthward are associated with the dipolarization of the stretched magnetic field line [see, e.g., *Nakamura et al.*, 2002; *Runov et al.*, 2011, 2012], also called dipolarization front (DF), that is embedded in these flows and separates the hot, tenuous high-speed flow from the cold, dense, and slowly convecting surrounding plasma. The typical scale of DFs in the near-Earth magnetotail is of the order of the ion inertial length and Larmor radius [see, e.g., *Runov et al.*, 2011; *Fu et al.*, 2012a].

DFs are invariably associated with intense and broadband electromagnetic fluctuations, from the ion cyclotron frequency to larger than the electron cyclotron frequency [see *Zhou et al.*, 2009; *Khotyaintsev et al.*, 2011; *Huang et al.*, 2012, 2015a; *Viberg et al.*, 2014, and references therein]. Various wave modes have been

identified, such as lower hybrid (LH) and whistler mode waves. While LH waves are observed directly at the DFs, whistler waves are generally detected in the flux pileup region (FPR), i.e., behind the DFs [*Khotyaintsev et al.*, 2011; *Deng et al.*, 2010; *Fu et al.*, 2014; *Li et al.*, 2015]. These waves, which are continually radiated outward from the BBFs to the auroral oval, are found to be a very efficient plasma sheet energy loss process [*Chaston et al.*, 2012; *Ergun et al.*, 2015], transferring the energy from the fields to the plasma [*Huang et al.*, 2015b; *Angelopoulos et al.*, 2013]. Whistlers have been previously recorded on board Cluster [*Khotyaintsev et al.*, 2011; *Huang et al.*, 2012] and Time History of Events and Macroscale Interactions during Substorms (THEMIS) [*Le Contel et al.*, 2009; *Deng et al.*, 2010] and are thought to be generated by the perpendicular electron temperature anisotropy resulting from betatron acceleration that occurs as the magnetic field strength increases inside the FPR [see, e.g., *Wu et al.*, 2013; *Fu et al.*, 2014; *Huang et al.*, 2015b; *Wu et al.*, 2015]. *Deng et al.* [2010] investigated the properties (namely, propagation angle, degree of polarization, and ellipticity) of whistler waves inside the magnetotail FPR, and by analyzing Poynting flux, *Khotyaintsev et al.* [2011] have shown that these waves are generated near the geomagnetic equator.

Recently, multispacecraft missions such as Cluster and THEMIS have allowed study of the detailed dynamics of BBFs. The fine structure of DFs has been investigated using the tetrahedron configuration of Cluster constellation by *Fu et al.* [2012b] [see also *Schmid et al.*, 2015]. They concluded that on a global-scale DFs are tangential discontinuities, although *Balikhin et al.* [2014] observed oscillations within a few DF magnetic ramps which would indicate field-aligned currents causing the plasma to flow across DFs. The radial separation along the magnetotail of the THEMIS fleet also helped to investigate the spatial evolution of BBFs [*Runov et al.*, 2009; *Sergeev et al.*, 2009]. In particular, *Runov et al.* [2009] showed [see also *Sitnov et al.*, 2009, 2013; *Fu et al.*, 2013; *Angelopoulos et al.*, 2013] that BBFs are consistent with magnetotail reconnection outflows, and thus, DFs originate from pulses of reconnection. Front-like structures may also appear due to the kinetic ballooning/interchange instability, forming finger-like structures [*Pritchett and Coroniti*, 2010, 2013; *Pritchett et al.*, 2014]. However, reconnection and interchange are not necessarily mutually exclusive, as the edge of a reconnection jet was shown to be interchange unstable [e.g., *Nakamura et al.*, 2002; *Runov et al.*, 2012], and localized reconnection could be triggered in the wake of interchange heads [*Pritchett and Coroniti*, 2011, 2013]. Nevertheless, the THEMIS interspacecraft separation distances are never smaller than the typical ion inertial length (~500 km) in the tail and do not allow study of the subprotonic dynamics of DFs.

In May 2015, the MMS [*Burch et al.*, 2016] constellation was in the near-Earth tail in a string-of-pearl configuration, with a very small separation distance ($\sim$ 160 km) between each spacecraft that allows us to study BBF propagation below ion scales. In this paper we take advantage of this unique configuration to investigate the spatial evolution of DFs on 15 May 2015 and their associated whistler emissions. In section 2 we first determine the propagation properties of the first DF, and then we show the low-frequency wave dynamics associated with this event. The results are discussed and summarized in section 3.

2. Data Analysis

Figure 1 gives an overview of the events observed on 15 May 2015 from 03:07:00 to 03:13:00 UT by the four MMS spacecraft located at (−11.7, 1.11, and 1.14) R_E in GSE coordinates. Because B_x is smaller than 10 nT, MMS was close to the magnetic equator. Only magnetic and electric field waveforms (all three components of each are obtained from digital fluxgate (DFG) [*Russell et al.*, 2016], axial double probe (ADP) [*Ergun et al.*, 2016], and spin-plane double probe (SDP) [*Lindqvist et al.*, 2016] instruments, respectively) as well as probe-to-spacecraft potential are presented in this figure, as the fast plasma investigation (FPI) [see *Pollock et al.*, 2016] instrument was turned off at this time during the commissioning phase. Two dipolarization events can be distinguished at about 03:08:10 and 03:11:55 UT, characterized by a steep magnetic ramp of the B_z component from −1 and 5 nT to 9 and 10 nT in about 8 and 5 s, respectively. The inclination of the magnetic field increases simultaneously of about 40 and 25°, respectively, and the maximum inclination angle is $\theta_{max} \geq 45°$ for both events. However, the first DF is accompanied by a high-speed flow ($v \geq 150$ km/s), whereas the second DF is not. For these two events, the behavior of the B_x component is similar (increase before and at the B_z ramp); however, it is opposite for B_y (B_y decreases at the second DF).

The variations of plasma density n, inferred from probe-to-spacecraft potential, are also opposite for the two DFs: the density increases slightly at the first DF (at 03:07:50 UT) but then decreases (fluctuations of $|B|$ and n are out of phase, as in fast modes), whereas at the second DF the density decreases at 03:11:50 UT and then increases behind the DF (fluctuations of $|B|$ and n are in phase, as in slow modes). These two types of density

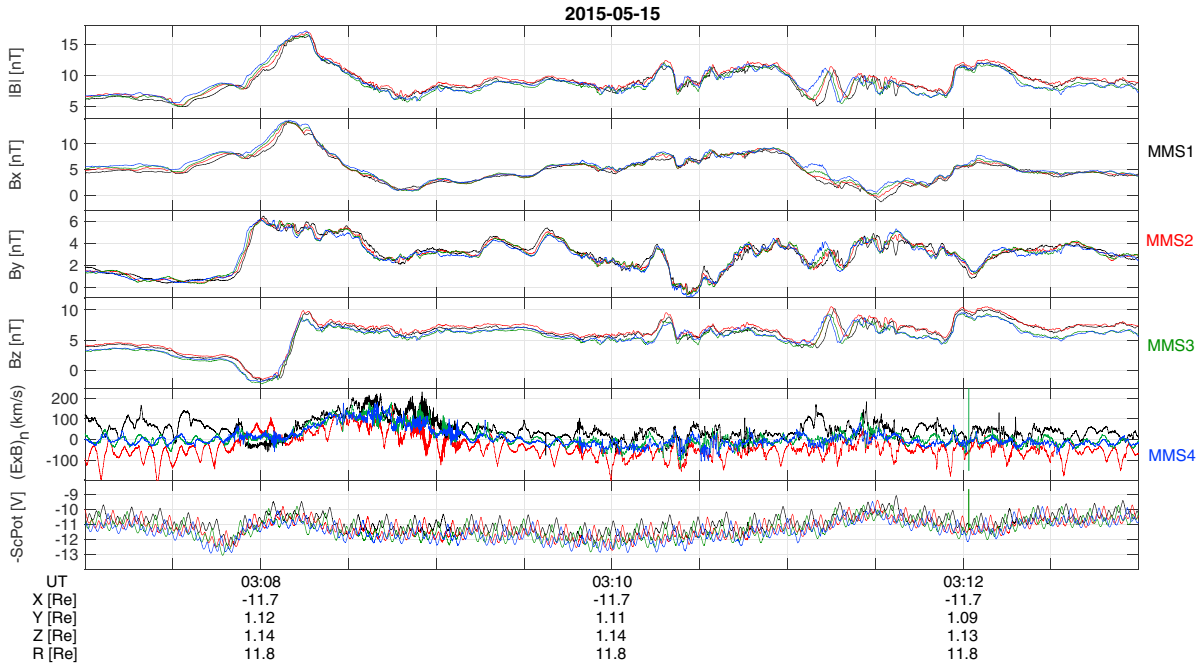

Figure 1. Summary of DFG and ADP/SDP measurements on board the four MMS spacecraft, on 15 May 2015 between 03:06:00 and 03:14:00 UT. From top to bottom panels are the modulus of magnetic field B, the x, y, and z components, the convected plasma velocity ($E \times B/B^2$) along the DF normal and the probe-to-spacecraft potential.

signatures have been observed in statistical studies [*Schmid et al.*, 2011, 2015], and the first DF seems to fall in categories A/D while the second DF falls in category B/C in the classification established by *Schmid et al.* [2015]. In addition, just before the first DF a very sharp potential (i.e., density) drop is observed, along with a decrease/increase of B_z/B_x resulting in a slight increase of $|B|$ ahead of the magnetic ramp (see Figure 1). These features are discussed in the following section.

We perform a minimum variance analysis (MVA) [see, e.g., *Sonnerup and Cahill*, 1967] at the two DFs for all spacecraft to determine the propagation properties of the normal to the front. The minimum variance directions (MVDs) calculated for the extent of the magnetic ramp of the first DF are (0.55, −0.83, 0.07), (0.48, −0.87, 0.05), (0.46, −0.88, 0.04), and (0.43, −0.9, 0.03) for MMS1, MMS2, MMS3, and MMS4, respectively. The MVDs for the first DF are well defined on all spacecraft with a ratio of the intermediate to minimum eigenvalues in the range (8–10) and a ratio of maximum to intermediate eigenvalues in the range (3–4). The normal of the first DF is thus mostly directed along Y. For the second DF the MVDs are less well defined; thus, in this paper we choose to study in detail the propagation properties of the first DF.

The normal to the first discontinuity (i.e., the direction of propagation of the first DF) derived from the MVA performed on each spacecraft is sketched in Figure 2. The normal of the first DF rotates significantly (the Y component decreases whereas the X and Z components increase) between each spacecraft in the XY and XZ planes, i.e., on a scale of $\sim$ 500 km, during its earthward propagation. In the absence of bulk plasma measurements, we determine the velocity of the convected plasma of the FPR (where the plasma is convected and the Hall term is small) [*Li et al.*, 2011; *Fu et al.*, 2012a] in the MVA frame as $(E \times B)/B^2 \approx 150$ km/s and directed along the minimum variance direction for the first DF (see Figure 1e). Assuming the duration of the front (i.e., the magnetic ramp) as $\Delta t \approx 8$ s (see the B_z component in Figure 1), we estimate the spatial scale (thickness) of the DF as $\Delta d \approx 1200$ km (i.e.,$\sim 2.5\rho_i$, ρ_i being the ion gyroradius). The standard timing analysis [see *Paschmann and Daly*, 1998, equation (12.9)] fails in our case (string-of-pearls configuration) because it requires the four spacecraft to be noncoplanar. However, the normals calculated for MMS4 and MMS3 are close to the plane determined by the alignment of the four spacecraft (see Figure 1), which is confirmed by the sequential observation of the DF by MMS4 and MMS3. The B_z profiles observed by MMS4 and MMS3 are also very similar, meaning we can do the timing unambiguously. Thus, by simply time shifting the B_z data from MMS4 and MMS3, we can estimate roughly the velocity of DF. We determine $\delta t \approx 1$ s between the two spacecraft, and thus, the velocity of the DF as $v_{DF} = \delta d/\delta t \approx 160$ km/s along the spacecraft separation, with an uncertainty of ~50 km/s.

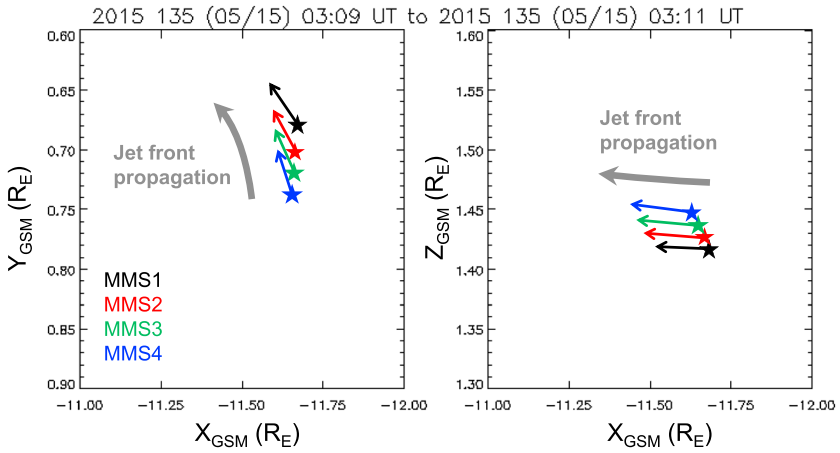

Figure 2. Sketch (not on scale) of the MVDs of the first DF obtained on board all four MMS spacecraft, in the equatorial (left) *XY* and meridional (right) *XZ* planes in GSM coordinates. The gray arrows depict the DF propagation inferred from the MVDs for the sake of clarity.

Taking into account the uncertainties on both velocity estimates ($E \times B/B^2$ and timing), the convective velocity and the discontinuity velocity can be considered as equal; therefore, the first DF can be characterized as a tangential discontinuity. These results and their probable causes are discussed in the following section.

We also perform an analysis of *E* and *B* fields fluctuations in the frequency range (1–64) Hz, i.e., between the ion and electron gyrofrequencies, obtained from ADP, SDP, and search-coil magnetometer (SCM) [*Le Contel et al.*, 2016] instruments. The results of this analysis for MMS2 are summarized in Figure 3. We observe very

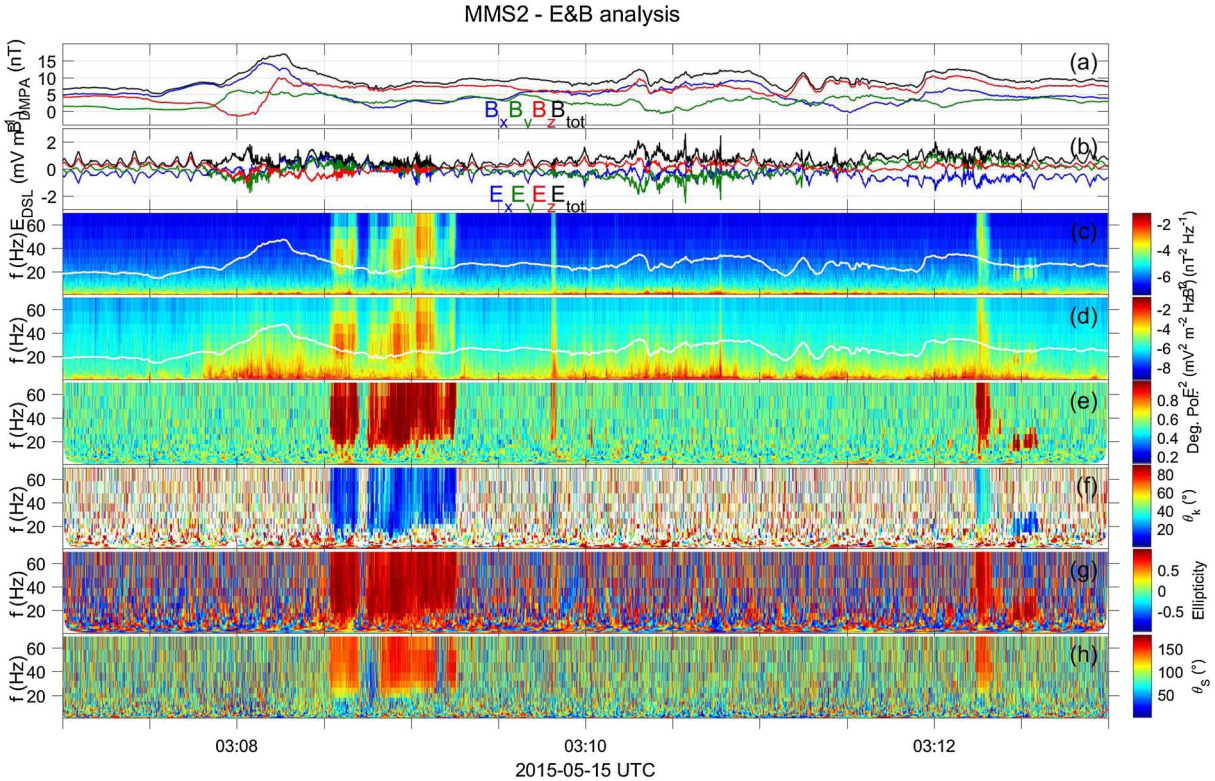

Figure 3. Example of detailed wave analysis performed on MMS2 in the frequency range (1–64) Hz: the (a) magnetic and (b) electric field waveforms from DFG and ADP/SDP instruments in Despun Major Principal Axis of inertia (DMPA) and Despun Spacecraft (DSL) coordinates, respectively, are color coded. (c and d) The time-frequency spectrograms computed from these waveforms. (e–h) The degree of polarization, propagation angle θ_k (between $\vec{k}$ and $\vec{B}_0$), ellipticity, and Poynting flux angle θ_S (between $\vec{S}$ and $\vec{B}_0$).

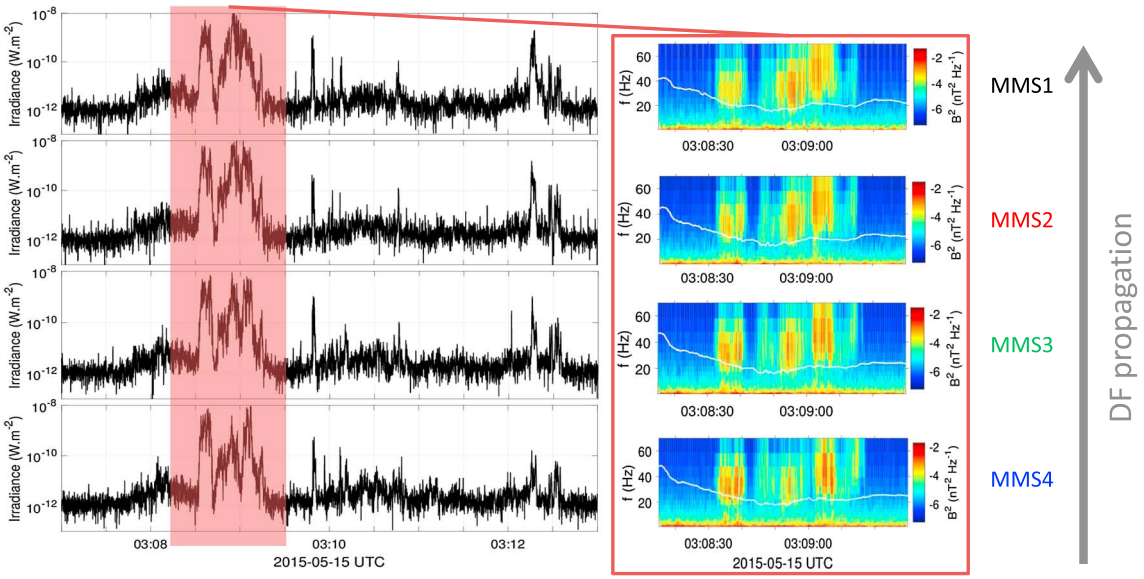

Figure 4. (left) The total electromagnetic power (irradiance), computed from the Poynting flux, is shown for all four spacecraft (from top to bottom MMS 1, 2, 3, and 4) along the DF propagation (gray arrow). (right) A zoom-in on 03:08:15 to 03:09:30 UT for each spacecraft shows the evolution of time-frequency spectrograms of whistler waves.

strong electrostatic fluctuations close to the lower hybrid (LH) frequency exactly at the time of the first DF (~03:08:10 UT). These are thus probably LH waves, as inherently observed at DFs [*Deng et al.*, 2010; *Khotyaintsev et al.*, 2011; *Huang et al.*, 2012]. Behind the first front we also observe strong electromagnetic fluctuations with a frequency just above $0.1f_{ce}$ (white line in Figure 3, f_{ce} being the electron gyrofrequency) and a highly (degree of polarization >0.9) right-handed (ellipticity ≈ 1) polarized, as well as a low propagation angle to the background magnetic field ($\theta \leq 20°$). Thus, these fluctuations are likely whistler waves, as often observed behind DFs [*Khotyaintsev et al.*, 2011; *Fu et al.*, 2014; *Viberg et al.*, 2014; *Li et al.*, 2015]. Weaker LH and whistler waves are also observed at and behind the second DF (~03:11:55 UT), which is also weaker in ΔB_z. However, the whistlers behind the second DF propagate obliquely ($\theta \approx 40-50°$) to the background magnetic field. In addition, although most of whistlers propagate toward the magnetic equator (antiparallel Poynting flux), we observe whistlers with a reversed Poynting flux (parallel to magnetic field) at about 03:08:45 UT, with less intensity as seen on magnetic and electric spectra. These results are discussed in the following section as well.

The same analysis was conducted on other spacecraft (not shown) resulting in similar wave properties (degree of polarization, wave angle, ellipticity, and Poynting flux) for this time interval. However, there is a clear evolution of magnetic spectra observed at the different spacecraft, as shown in Figure 4. The latter displays enhanced magnetic fluctuations along the BBFs trajectory so that MMS1 (which is closer to the Earth, see Figure 2) observes strong whistlers at 03:08:55 UT, whereas MMS4 does not. Whistlers behind the second DF are also stronger on MMS1 than on MMS4 (see Figure 4). This wave growth enhances the electromagnetic power by about 2 orders of magnitude (from about 2.10^{-10} on MMS4 to 1.10^{-8} W/m^2 on MMS1) behind the first DF and about 1 order of magnitude (from $\sim 1.10^{-10}$ to 1.10^{-9} W/m^2) behind the second DF, as seen on Figure 4. Figure 4 also shows that quasi-parallel whistlers at 03:08:55 UT are (about 1 order of magnitude) less intense than antiparallel ones.

3. Summary and Discussion

In May 2015, the newly launched MMS fleet was orbiting Earth in a string-of-pearls configuration. For the first time such configuration with very close spacecraft separation distance (~ 160 km) flew through the near-Earth magnetotail (~10–12 R_E). Making use of this unique opportunity, in this study we investigate the small-scale (i.e., below the ion gyroradius) dynamics of DFs propagation in the tail and their associated low-frequency emissions.

Our results can be summarized as follows. (1) Two DF structures are identified, both generated at the magnetic equator and propagating earthward, but they are probably of different nature: based on the density variations therein, they fall into different categories of DFs [*Schmid et al.*, 2015]. (2) The first DF is probably a tangential discontinuity and is very dynamic: its normal rotates toward Earth on spatial scales less than the ion gyroradius (~500 km). (3) Both DFs show strong associated low-frequency waves (LH at DF and whistlers behind it) but with different properties: while intense quasi-parallel whistlers are observed behind the first DF, weaker oblique whistlers are observed behind the second one. (4) The dynamics of whistler waves associated with the first DF are also subprotonic: in less than 2 s $|B|$ increases (i.e., the flux tube is compressed) as the DF propagates earthward (from MMS4 to MMS1) and the whistler electromagnetic power is enhanced by 1 to 2 orders of magnitude. Some wave packets are observed to have a reversed (antiparallel) Poynting flux within the FPR. However, these results raise some questions that we discuss in the following paragraph.

As deduced from the MVA, the two DF events in this study seem to be generated in the midtail (they propagate earthward) at the magnetic equator, in agreement with models [*Runov et al.*, 2011; *Sitnov et al.*, 2013; *Nakamura et al.*, 2002; *Pritchett et al.*, 2014] and previous observations [e.g., *Le Contel et al.*, 2009]. The normal of the first DF is first directed dawnward (*XY* plane) but then rotates earthward (*Y* component decreases, while *X* and *Z* components increase) during its propagation, on a spatial scale (~500 km) less than the ion gyroradius. This subprotonic-scale rotation of the DF might, for instance, modify the dynamics of accelerated high-energy particles in the vicinity of the DF (such as, for instance, reflected ions ahead of the DF as described in *Zhou et al.* [2010]). Detailed analysis of such particle measurements using MMS data and dedicated numerical simulations is thus necessary to determine the effects on particle dynamics at these scales. The MVDs calculated for the first front are clearly defined, in contrast with the MVDs calculated for the second DF; presumably because the second DF is located in the "turbulent trail" of the first DF, as the magnetic field from ~03:09:50 to 03:12:00 UT appears to be highly fluctuating. Nevertheless, particle measurements are needed to study turbulence in the vicinity of DF [*Huang et al.*, 2012] and in BBFs [*Vörös et al.*, 2004, 2006], and this issue is thus beyond the scope of this study.

The estimation of the bulk plasma, as deduced from $(E \times B)/B^2$) and discontinuity (roughly estimated from timing analysis) velocities give rather similar values (~150 km/s), and the bulk velocity is directed along the front normal; thus, this DF seems to be a tangential discontinuity [*Schmid et al.*, 2011; *Fu et al.*, 2012b]. Additionally, fluctuations in the magnetic ramp are weak; thus, field-aligned currents at the DF must not be strong, and the plasma flow crossing the instability may not be significant [*Balikhin et al.*, 2014; *Huang et al.*, 2015b]. In addition, a significant drop in density (inferred from probe-to-spacecraft potential) over about 20 s is observed about 30 s ahead of the first DF (at ~03:07:35). This steep density hole is accompanied by a singular magnetic signature (slight increase in B_x and decrease in B_z components, see Figure 1), whereas no particular electric fluctuations are observed at this time (e.g., on MMS2, see Figure 3). This could be the signature of the earthward propagation of a DF as a flux rope, as depicted in the multiple reconnection *X* lines model [see, e.g., *Lee*, 1995; *Slavin et al.*, 2003; *Huang et al.*, 2015; *Lu et al.*, 2015]. In particular, *Lu et al.* [2015] have performed a 3-D hybrid simulation of DFs as earthward propagating flux ropes and have shown that the multiple X line reconnection process gives rise to flux ropes that propagate earthward with a B_z and plasma density dip signature (as observed on Figure 1) ahead of them [see *Lu et al.*, 2015, Figures 1b–1e], especially if a previously formed flux rope is located closer to the Earth [see *Lu et al.*, 2015, Figure 1c]. However, the exact nature of this phenomenon is still to be determined, and we leave this for future studies.

Intense low-frequency waves are also observed at (LH) and behind (whistlers) DFs. The calculation of Poynting flux (see Figure 3) seems to indicate that they propagate toward the magnetic equator. However, the presence of the two sudden reversals in their direction of propagation and the fact that B_x oscillates around zero when they are observed suggest that the spacecraft are located in the whistler generation region close to the magnetic equator [*Le Contel et al.*, 2009; *Runov et al.*, 2011]. This propagation direction is consistent with the position of the spacecraft at that time ($Z_{GSE} \approx 1.14 R_E$). Whistlers become more intense closer to the Earth as $|B|$ increases from MMS4 to MMS1 when they are observed (i.e., the flux tube is compressed), indicating that the perpendicular anisotropy may vary at the time scale of the ion gyroperiod (~2 s). From Figure 4 a very rough estimation of the growth rate gives $\gamma \approx 0.001\Omega_e$, $\Omega_e \approx 200$ Hz being the electron gyropulsation (see Figure 4 (right)). This result is consistent with growth rates calculated from models with similar plasma parameters (see, e.g., first plasma model from *Le Contel et al.* [2009]). However, to accurately determine the temperature anisotropy, data particle is needed, and thus this issue is beyond the scope of the present study.

Whereas the whistlers at the first DF are quasi-parallel, those observed behind the second front are oblique to the magnetic field. As stated above, the estimation of density variations indicate that according to *Schmid et al.* [2015] classification, the two DFs in this study may be of different nature. Thus, it might be possible that the properties of whistlers associated with DFs are dependent on the nature of these DFs, as different pitch angle distributions of suprathermal electrons have been observed behind different types of DFs [*Fu et al.*, 2011, 2012c]. However, a statistical study of low-frequency emissions associated to DFs of different nature is necessary and is left for future investigation.

To conclude, the subprotonic dynamics of DFs (rotation of the normal on a scale ~500 km) and their associated low-frequency emissions (whistler waves intensification) in the magnetotail are shown for the first time due to the small separation distance (~160 km) of MMS string-of-pearls configuration in May 2015. Unfortunately, the FPI instruments were not turned on at that time so only electromagnetic fields data are presented. Observations in phase 1X (starting in March 2016) will also have FPI instruments turned on very sparsely and moreover the apogee in the nightside will be located far from the magnetic equator ($Z \approx 5R_E$). Thus, the events shown in this paper represent a unique opportunity to study the kinetic-scale dynamics of DF propagation and associated whistler emissions.

Acknowledgments
H.B.'s work has been supported by CNES through the grant "Allocations de recherche post-doctorale." The French involment (SCM) on MMS is supported by CNES, CNRS-INSIS, and CNRS-INSU. Used data are available at https://lasp.colorado.edu/mms/sdc.

References

Angelopoulos, V., A. Runov, X.-Z. Zhou, D. L. Turner, S. A. Kiehas, S.-S. Li, and I. Shinohara (2013), Electromagnetic energy conversion at reconnection fronts, *Science*, *341*(6153), 1478–1482, doi:10.1126/science.1236992.

Balikhin, M. A., A. Runov, S. N. Walker, M. Gedalin, I. Dandouras, Y. Hobara, and A. Fazakerley (2014), On the fine structure of dipolarization fronts, *J. Geophys. Res. Space Physics*, *119*, 6367–6385, doi:10.1002/2014JA019908.

Baumjohann, W. (1993), The near Earth plasma sheet–An AMPTE/IRM perspective, *Space Sci. Rev.*, *64*, 141–163, doi:10.1007/BF00819660.

Baumjohann, W., R. Schödel, and R. Nakamura (2002), Bursts of fast magnetotail flux transport, *Adv. Space Res.*, *30*, 2241–2246, doi:10.1016/S0273-1177(02)80234-4.

Burch, J. L., T. E. Moore, R. B. Torbert, and B. L. Giles (2016), Magnetospheric multiscale overview and science objectives, *Space Sci. Rev.*, *199*(1), 5–21, doi:10.1007/s11214-015-0164-9.

Chaston, C. C., J. W. Bonnell, L. Clausen, and V. Angelopoulos (2012), Energy transport by kinetic-scale electromagnetic waves in fast plasma sheet flows, *J. Geophys. Res.*, *117*, A09202, doi:10.1029/2012JA017863.

Deng, X., M. Ashour-Abdalla, M. Zhou, R. Walker, M. El-Alaoui, V. Angelopoulos, R. E. Ergun, and D. Schriver (2010), Wave and particle characteristics of earthward electron injections associated with dipolarization fronts, *J. Geophys. Res.*, *115*, A09225, doi:10.1029/2009JA015107.

Ergun, R. E., K. A. Goodrich, J. E. Stawarz, L. Andersson, and V. Angelopoulos (2015), Large-amplitude electric fields associated with bursty bulk flow braking in the Earth's plasma sheet, *J. Geophys. Res. Space Physics*, *120*, 1832–1844, doi:10.1002/2014JA020165.

Ergun, R. E., et al. (2016), The axial double probe and fields signal processing for the mms mission, *Space Sci. Rev.*, *199*(1), 167–188, doi:10.1007/s11214-014-0115-x.

Fu, H. S., Y. V. Khotyaintsev, M. André, and A. Vaivads (2011), Fermi and betatron acceleration of suprathermal electrons behind dipolarization fronts, *Geophys. Res. Lett.*, *38*, L16104, doi:10.1029/2011GL048528.

Fu, H. S., Y. V. Khotyaintsev, A. Vaivads, M. André, and S. Y. Huang (2012a), Occurrence rate of earthward-propagating dipolarization fronts, *Geophys. Res. Lett.*, *39*, L10101, doi:10.1029/2012GL051784.

Fu, H. S., Y. V. Khotyaintsev, A. Vaivads, M. André, and S. Y. Huang (2012b), Electric structure of dipolarization front at sub-proton scale, *Geophys. Res. Lett.*, *39*, L06105, doi:10.1029/2012GL051274.

Fu, H. S., Y. V. Khotyaintsev, A. Vaivads, M. André, V. A. Sergeev, S. Y. Huang, E. A. Kronberg, and P. W. Daly (2012c), Pitch angle distribution of suprathermal electrons behind dipolarization fronts: A statistical overview, *J. Geophys. Res.*, *117*, A12221, doi:10.1029/2012JA018141.

Fu, H. S., et al. (2013), Dipolarization fronts as a consequence of transient reconnection: In situ evidence, *Geophys. Res. Lett.*, *40*, 6023–6027, doi:10.1002/2013GL058620.

Fu, H. S., et al. (2014), Whistler-mode waves inside flux pileup region: Structured or unstructured?, *J. Geophys. Res. Space Physics*, *119*, 9089–9100, doi:10.1002/2014JA020204.

Huang, S. Y., M. Zhou, X. H. Deng, Z. G. Yuan, Y. Pang, Q. Wei, W. Su, H. M. Li, and Q. Q. Wang (2012), Kinetic structure and wave properties associated with sharp dipolarization front observed by cluster, *Ann. Geophys.*, *30*(1), 97–107, doi:10.5194/angeo-30-97-2012.

Huang, S. Y., et al. (2012), Observations of turbulence within reconnection jet in the presence of guide field, *Geophys. Res. Lett.*, *39*, L11104, doi:10.1029/2012GL052210.

Huang, S. Y., et al. (2015a), Observations of large-amplitude electromagnetic waves and associated wave-particle interactions at the dipolarization front in the Earth's magnetotail: A case study, *J. Atmos. Sol. Terr. Phys.*, *129*, 119–127, doi:10.1016/j.jastp.2015.05.007.

Huang, S. Y., et al. (2015b), Electromagnetic energy conversion at dipolarization fronts: Multispacecraft results, *J. Geophys. Res. Space Physics*, *120*, 4496–4502, doi:10.1002/2015JA021083.

Huang, S. Y., et al. (2015), Kinetic simulations of secondary reconnection in the reconnection jet, *J. Geophys. Res. Space Physics*, *120*, 6188–6198, doi:10.1002/2014JA020969.

Juusola, L., N. ØStgaard, E. Tanskanen, N. Partamies, and K. Snekvik (2011), Earthward plasma sheet flows during substorm phases, *J. Geophys. Res.*, *116*, A10228, doi:10.1029/2011JA016852.

Khotyaintsev, Y. V., C. M. Cully, A. Vaivads, M. André, and C. J. Owen (2011), Plasma jet braking: Energy dissipation and nonadiabatic electrons, *Phys. Rev. Lett.*, *106*, 165001, doi:10.1103/PhysRevLett.106.165001.

Le Contel, O., et al. (2009), Quasi-parallel whistler mode waves observed by THEMIS during near-Earth dipolarizations, *Ann. Geophys.*, *27*(6), 2259–2275, doi:10.5194/angeo-27-2259-2009.

Le Contel, O., et al. (2016), The search-coil magnetometer for MMS, *Space Sci. Rev.*, *199*, 257–282, doi:10.1007/s11214-014-0096-9.

Lee, L. C. (1995), *A Review of Magnetic Reconnection: MHD Models*, AGU, Washington, D. C.

Li, H., M. Zhou, X. Deng, Z. Yuan, L. Guo, X. Yu, Y. Pang, and S. Huang (2015), A statistical study on the whistler waves behind dipolarization fronts, *J. Geophys. Res. Space Physics*, *120*, 1086–1095, doi:10.1002/2014JA020474.

Li, W., J. Bortnik, R. M. Thorne, and V. Angelopoulos (2011), Global distribution of wave amplitudes and wave normal angles of chorus waves using THEMIS wave observations, *J. Geophys. Res.*, *116*, A12205, doi:10.1029/2011JA017035.
Lindqvist, P.-A., et al. (2016), The spin-plane double probe electric field instrument for MMS, *Space Sci. Rev.*, *199*(1), 137–165, doi:10.1007/s11214-014-0116-9.
Lu, S., Q. Lu, Y. Lin, X. Wang, Y. Ge, R. Wang, M. Zhou, H. Fu, C. Huang, M. Wu, and S. Wang (2015), Dipolarization fronts as earthward propagating flux ropes: A three-dimensional global hybrid simulation, *J. Geophys. Res. Space Physics*, *120*, 6286–6300, doi:10.1002/2015JA021213.
Nakamura, M. S., H. Matsumoto, and M. Fujimoto (2002), Interchange instability at the leading part of reconnection jets, *Geophys. Res. Lett.*, *29*, 1247, doi:10.1029/2001GL013780.
Ohtani, S.-I., M. A. Shay, and T. Mukai (2004), Temporal structure of the fast convective flow in the plasma sheet: Comparison between observations and two-fluid simulations, *J. Geophys. Res.*, *109*, A03210, doi:10.1029/2003JA010002.
Paschmann, G., and P. W. Daly (1998), Analysis methods for multi-spacecraft data, *1*.
Pollock, C., et al. (2016), Fast plasma investigation for magnetospheric multiscale, *Space Sci. Rev.*, *199*, 331–406, doi:10.1007/s11214-016-0245-4.
Pritchett, P. L., and F. V. Coroniti (2010), A kinetic ballooning/interchange instability in the magnetotail, *J. Geophys. Res.*, *115*, A06301, doi:10.1029/2009JA014752.
Pritchett, P. L., and F. V. Coroniti (2011), Plasma sheet disruption by interchange-generated flow intrusions, *Geophys. Res. Lett.*, *38*, L10102, doi:10.1029/2011GL047527.
Pritchett, P. L., and F. V. Coroniti (2013), Structure and consequences of the kinetic ballooning/interchange instability in the magnetotail, *J. Geophys. Res. Space Physics*, *118*, 146–159, doi:10.1029/2012JA018143.
Pritchett, P. L., F. V. Coroniti, and Y. Nishimura (2014), The kinetic ballooning/interchange instability as a source of dipolarization fronts and auroral streamers, *J. Geophys. Res. Space Physics*, *119*, 4723–4739, doi:10.1002/2014JA019890.
Runov, A., V. Angelopoulos, M. I. Sitnov, V. A. Sergeev, J. Bonnell, J. P. McFadden, D. Larson, K.-H. Glassmeier, and U. Auster (2009), THEMIS observations of an earthward-propagating dipolarization front, *Geophys. Res. Lett.*, *36*, L14106, doi:10.1029/2009GL038980.
Runov, A., et al. (2011), Dipolarization fronts in the magnetotail plasma sheet, *Planet. Space Sci.*, *59*, 517–525, doi:10.1016/j.pss.2010.06.006.
Runov, A., V. Angelopoulos, and X.-Z. Zhou (2012), Multipoint observations of dipolarization front formation by magnetotail reconnection, *J. Geophys. Res.*, *117*, A05230, doi:10.1029/2011JA017361.
Russell, C. T., et al. (2016), The magnetospheric multiscale magnetometers, *Space Sci. Rev.*, *199*(1), 189–256, doi:10.1007/s11214-014-0057-3.
Schmid, D., M. Volwerk, R. Nakamura, W. Baumjohann, and M. Heyn (2011), A statistical and event study of magnetotail dipolarization fronts, *Ann. Geophys.*, *29*(9), 1537–1547, doi:10.5194/angeo-29-1537-2011.
Schmid, D., R. Nakamura, F. Plaschke, M. Volwerk, and W. Baumjohann (2015), Two states of magnetotail dipolarization fronts: A statistical study, *J. Geophys. Res. Space Physics*, *120*, 1096–1108, doi:10.1002/2014JA020380.
Sergeev, V., V. Angelopoulos, S. Apatenkov, J. Bonnell, R. Ergun, R. Nakamura, J. McFadden, D. Larson, and A. Runov (2009), Kinetic structure of the sharp injection/dipolarization front in the flow-braking region, *Geophys. Res. Lett.*, *36*, L21105, doi:10.1029/2009GL040658.
Sitnov, M. I., M. Swisdak, and A. V. Divin (2009), Dipolarization fronts as a signature of transient reconnection in the magnetotail, *J. Geophys. Res.*, *114*, A04202, doi:10.1029/2008JA013980.
Sitnov, M. I., N. Buzulukova, M. Swisdak, V. G. Merkin, and T. E. Moore (2013), Spontaneous formation of dipolarization fronts and reconnection onset in the magnetotail, *Geophys. Res. Lett.*, *40*, 22–27, doi:10.1029/2012GL054701.
Slavin, J. A., R. P. Lepping, J. Gjerloev, D. H. Fairfield, M. Hesse, C. J. Owen, M. B. Moldwin, T. Nagai, A. Ieda, and T. Mukai (2003), Geotail observations of magnetic flux ropes in the plasma sheet, *J. Geophys. Res.*, *108*, 1015, doi:10.1029/2002JA009557.
Sonnerup, B. U. ., and L. J. Cahill (1967), Magnetopause structure and attitude from explorer 12 observations, *J. Geophys. Res.*, *72*(1), 171–183, doi:10.1029/JZ072i001p00171.
Viberg, H., Y. V. Khotyaintsev, A. Vaivads, M. André, H. S. Fu, and N. Cornilleau-Wehrlin (2014), Whistler mode waves at magnetotail dipolarization fronts, *J. Geophys. Res. Space Physics*, *119*, 2605–2611, doi:10.1002/2014JA019892.
Volwerk, M., et al. (2008), Magnetotail dipolarization and associated current systems observed by Cluster and Double Star, *J. Geophys. Res.*, *113*, A08S90, doi:10.1029/2007JA012729.
Vörös, Z., W. Baumjohann, R. Nakamura, M. Volwerk, and A. Runov (2006), Bursty bulk flow driven turbulence in the Earth's plasma sheet, *Space Sci. Rev.*, *122*, 301–311, doi:10.1007/s11214-006-6987-7.
Vörös, Z., et al. (2004), Magnetic turbulence in the plasma sheet, *J. Geophys. Res.*, *109*, A11215, doi:10.1029/2004JA010404.
Wu, M., M. Volwerk, Q. Lu, Z. Vörös, R. Nakamura, and T. Zhang (2013), The proton temperature anisotropy associated with bursty bulk flows in the magnetotail, *J. Geophys. Res. Space Physics*, *118*, 4875–4883, doi:10.1002/jgra.50451.
Wu, M., C. Huang, Q. Lu, M. Volwerk, R. Nakamura, Z. Vörös, T. Zhang, and S. Wang (2015), In situ observations of multistage electron acceleration driven by magnetic reconnection, *J. Geophys. Res. Space Physics*, *120*, 6320–6331, doi:10.1002/2015JA021165.
Zhou, M., M. Ashour-Abdalla, X. Deng, D. Schriver, M. El-Alaoui, and Y. Pang (2009), THEMIS observation of multiple dipolarization fronts and associated wave characteristics in the near-Earth magnetotail,*Geophys. Res. Lett.*, *36*, L20107, doi:10.1029/2009GL040663.
Zhou, X.-Z., V. Angelopoulos, V. A. Sergeev, and A. Runov (2010), Accelerated ions ahead of earthward propagating dipolarization fronts, *J. Geophys. Res.*, *115*, A00I03, doi:10.1029/2010JA015481.